Canadian Science Publishing | Transactions of the Canadian Society for Mechanical Engineering

Effect of welding parameters on mechanical and corrosion behavior of stellite 6 cladded SA387 Gr 91 with ERNiCr-3 buffer layer

Journal:	*Transactions of the Canadian Society for Mechanical Engineering*
Manuscript ID	TCSME-2019-0277.R1
Manuscript Type:	Article
Date Submitted by the Author:	03-Jan-2020
Complete List of Authors:	Britto Joseph, G.; Sathyambama Institute of Science and Technology, school of mechanical engineering T.N., Valarmathi; Sathyambama Institute of Science and Technology, school of mechanical engineering A, John Rajan; Vellore Institute of Technology
Keywords:	SA387 Gr 91, ERNiCr-3, Stellite 6, Robotic welding, hardness
Is the invited manuscript for consideration in a Special Issue? :	Not applicable (regular submission)

EFFECT OF WELDING PARAMETERS ON MECHANICAL AND CORROSION BEHAVIOR OF STELLITE 6 CLADDED SA387 GR 91 WITH ERNICR-3 BUFFER LAYER

G Britto Joseph[1], T. N Valarmathi[2]*, A John Rajan[3]

[1]*Research Scholar, School of Mechanical Engineering, Sathyabama Institute of Science and Technology, Chennai, India*

[2]*Associate Professor, School of Mechanical Engineering, Sathyabama Institute of Science and Technology, Chennai, India*

[3]*, Professor, Department of Manufacturing Engineering, VIT, Vellore*

E-mail: workbritto@gmail.com, valarmathi.tn@gmail.com

ABSTRACT

The mechanical, chemical and corrosion properties of the cladded material strongly depend upon the geometry of clad beads. Hence it is essential to learn the impact of process parameters on the weld bead geometry. In this work, the effects of welding speed (WS), welding current (WC) and nozzle to plate (PD) distance on cladding are investigated in terms of improving the mechanical and corrosion properties. SA387 Gr 91 is cladded with stellite 6 as cladding material and ERNiCr-3 as a buffer layer by IRB1520 ID Robotic welding. The experiments are carried out using three factors with three levels as per Box-Behnken design technique. The characterization study is made using optical microscope and Scanning electron microscope (SEM). The hardness is measured using Vicker's hardness tester. Electrochemical corrosion test is conducted in order to determine the corrosion resistance. The application of ERNiCr-3 reduces the cracks and pores on the surface of the cladded metal. Among the chosen parameters, welding current is the most important parameter controlling the mechanical and corrosion properties. From the results, it is concluded that the combination of ERNiCr-3 and Stellite 6 enhances the corrosion resistance and mechanical properties of SA387 Gr 91 significantly.

Keywords: SA387 Gr 91; ERNiCr-3; Stellite 6; Robotic welding; hardness.

1. Introduction

Stainless steel is widely used in engineering applications because of its high corrosion resistance. On the stainless steel, Stellite 6 material mostly overlaid for frequently operating valve seated rings and valve wedges application which is withstand for high temperature and high pressure. The properties of the Stellite 6 not only increases the corrosion resistance but also increases the wear resistance in hot corrosive environment. Dissimilar overlaying is a technique, which would increase the corrosion resistance and wear resistance characteristics of the base metal without disturbing its characteristics even at high pressure and high temperature (Mohammed MohaideenFerozhkhan et al. 2017). Many attracting characteristics of the Stellite 6 are abrasion resistance, galling resistance, corrosion resistance, oxidation resistance and wear resistance at atmospheric condition and hot environment (Mohammed MohaideenFerozhkhan et al. 2016). The chemical compositions of Stellite 6 are tungsten, cobalt, chromium and carbon, which form a carbides Co-Cr. This Co-Cr solid solution strengthening the nonferrous alloying matrix (SerkanApay and BehcetGulenc 2016). Results of dispersing carbides inside cobalt alloy matrix, it leads to increase the characteristics of high hardness and high strength of the Stellite 6 (ArabiJeshvaghani. R et al. 2011). $M_{23}C_6$ and M_7C_3 carbides formation increases the strength of chromium at high temperature and also increases the oxidization resistance and corrosion resistance of the metal (Deng D. W. et al. 2012). Several welding methods for example tungsten inert gas (TIG) welding, shielded metal arc welding (SMAW), laser cladding process and plasma transfer arc welding (PAW) are used for overlaying the Stellite 6 on base metals. Normally, the overlaying of the Stellite 6 depends on the manufacturing cost, productivity, design of weld bead, base metal and welding parameters.

(Hajiannia et al. 2019) carried various experimental work to weld the low alloy steel and stainless steel by GTAW process using ER309L and ERNiCr-3 fillers. The consequences of those tests indicated that the the filler ERNiCr-3 exhibit good mechanical properties and metallurgical properties than the ER309L filler welding.On SA 387 Gr 91, Stellite 6 cannot be directly overlaid, because of its sensitivity characteristics. Directly overlaying the Stellite 6 on SA 387 Gr 91, leads to more iron content and admixture of Stellite 6 alloy in base metal. More iron content and admixture of Stellite 6 alloys affects the

base metal properties and leads to cracks on HAZ and weldment area and also it reduces the chromium content in grain boundaries (Tian H. L. et al 2014). In order to overcome these problems, the buffer layer should be introduced in between SA 387 Gr 91 and Stellite 6. Formation of martensite, and its hardness in welded area also decides the quality of the weld. To prevent the formation of the martensite, the various buffers generally used for higher temperature applications. Several research works have been conducted by using Stellite 6 overlay on different base metals to improve the wear resistance and corrosion resistance (SerkanApay and BehcetGulenc 2016). So far, ER NiCr-3 buffer layer has not been considered in literatures for overlaying Stellite 6 on SA 387 Gr 91 base metal for higher temperature application. The aim of this work is to study the weld parameters closer to the optimum values by introducing ER NiCr-3 buffer layer and then overlaying the Stellite 6 on the ER NiCr-3 layer for enabling the corrosion resistance and good mechanical properties.

2. Experimental work

SA 387 Gr 91, ERNiCr-3 and Stellite 6 are purchased from the different sources through Indiamart. The chemical composition of SA 387 Gr 91, ERNiCr-3 and Stellite 6 are given in table 1. Before cladding, the SA 387 grade 91 base metal samples of 200 x 100 x 15mm are cleaned to remove dust, oil and other impurities, and preheated to 220^0C. The ERNiCr-3 filler of diameter 1.6 mm is first deposited over the base metal SA 387 gr 91surface by 5 mm, and is grounded to 3 mm by surface grinding machine. This welded piece is forwarded to post weld heat treatment (at 745^0C and for 1 hour). The welded piece is again preheated to 220^0C, and Stellite-6 is then cladded using the IRB1520 ID six axis robotic welding machine. The range of welding parameters is mention in table 2. The design matrices for ERNiCr-3 and Stellite 6 are given in table 3.

2. Experimental design procedure

a. Finding the input parameters

There are many welding parameters that influence the quality of the weld. Among all the welding parameters, the selected welding parameters are WC, WS and PD and selected responses are weld bead, reinforcement, depth of penetration and form factor.

b.Finding the range of input parameters

The range of all the welding parameters has been determined by considering one parameter being fixed and varying remaining all the parameters. To determine the approximate range of welding parameters, few trail runs are conducted. Equation 1 is used for determining the ranges of welding parameters [7].

$$\text{Ki} = \frac{2(2K - [Kmax + Kmin])}{Kmax - Kmin} \quad (1)$$

Where *Ki* is the desired coded value of a parameter *K*. *K* is the value of the welding parameter from *Kmin* to *Kmax*, where *Kmin* is the lower boundary of the welding parameter and *Kmax* is the upper boundary of the welding parameter. The selected welding parameters are given in table 2.

c. **Recording the response variables**

Crosswise section areas of individual weld overlay are cut utilizing a power hacksaw from mid-length location of the welds, and the appearances of the cut location are machined. These samples are set up by the typical metallurgical cleaning strategies and polished with 2% nital according to the procedure described by Deng et al. [5]. The weld bead profiles are followed utilizing an optical profile projector at an amplification of 10. The profile pictures are stored in AutoCAD 2004 package as raster picture, and profiles are followed in 2D structure. From the 2D chart, the penetration, reinforcement, and weld bead width are estimated. The shape connections in reinforcement shape factor (shape factor = weld bead width/height of reinforcement) are determined.

d.Determination of regression coefficient and mathematical development

Equation (2) represents the response of the weld bead profile [8].

$$X = f(WC, WS, PD) \quad (2)$$

Where X – response: WC – Welding current; WS – Welding speed; PD – Nozzle to plate distance

The second order polynomial equation used for the 3 factors can be characterized by the Equation (3) [9].

$$Z=K_0+K_1WC+K_2WS+K_3PD+K_{11}WC^2+K_{22}WS^2+K_{33}WD^2+K_{12}WCWS+K_{23}WSWD+K_{13}WCWD \quad (3)$$

Where K_0 - free coefficient of polynomial equation. K_1, K_2 and K_3 – linear terms of polynomial equation. K_{11}, K_{22} and K_{33} – quadratic equation of polynomial equation. K_{12}, K_{13} and K_{23} – interaction terms of polynomial equation.

e. **Determination of co efficient**

The estimations of the coefficients of the above polynomial mentioned in equation (3) are calculated with the aid of a Response surface methodology. The evaluated coefficients are mention in Table 4.

f. ANOVA

The evaluated coefficients are utilized to build the model for the response parameter. The effectiveness of the model which is developed is then checked by ANOVA (analysis of variance) method as shown in Table 5. It is revealed that the determined F proportions are bigger than the organized qualities at 95% certainty level; subsequently the model is viewed as satisfactory [10]. One more basis that is regularly used to represent the sufficiency of a fitted regression model is the coefficient of regression (R^2) and balanced R^2. For the models built up the determined R^2 and balanced R^2 qualities are given in Table 5. These qualities show that the regression models are very satisfactory.

g. Development of final mathematical models

The developed mathematical models of responses are listed below in the coded form.

$$P_E = 1.05+0.095WC-0.06WS-0.03PD-0.012WCWS-0.05WCPD-0.024WSPD-0.063WC^2- 0.044WS^2-0.062PD^2 \quad (4)$$

$$R_E = 4.32+0.16WC-0.2WS+ 0.02PD-0.03WCWS–0.008WCPD+0.009WSPD+0.017WC^2+0.013WS^2+0.052PD^2 \quad (5)$$

$$W_E = 10.73+1.48WC-0.42WS-0.090PD+0.17WCWS-0.42WCPD+0.18WSPD-0.13WC^2-0.076WS^2 +0.36PD^2 \quad (6)$$

$$FF_E = 2.48+0.25WC+0.02WS-0.04PD+0.065WCWS-0.09WCPD+0.04WSPD-0.05WC^2-0.021WS^2+0.051PD^2 \quad (7)$$

$$P_S = 1.05+0.1WC-0.06WS-0.04PD – 0.01WCWS-0.051WCPD-0.022WSPD-0.058WC^2-0.043WS^2-0.072PD^2 \quad (8)$$

$$R_S = 4.32+0.18WC-0.20WS+0.03PD-0.03WCWS-0.01WCPD+ 0.007WSPD +0.02WC^2 +0.013WS^2 +0.05PD^2 \quad (9)$$

$$W_S = 10.75+1.51WC-0.40WS-0.063PD+0.13WCWS-0.44WCPD+0.15SPD-0.15WC^2-0.091WS^2 +0.37PD^2 \quad (10)$$

$$FF_S = 2.49+0.24WC+0.024WS-0.03PD+0.06WCWS-0.10WCPD+0.03WSPD-0.052WC^2-0.021\ WS^2+0.04PD^2 \quad (11)$$

h. Scatter Diagram

The validity of the regression models created are additionally checked by using scatter graphs. A typical scatter diagram is shown in figure 1. The observed values and predicted estimations of the experiments are dissipated near the 45° line, showing that the values are closer to the experimental model [11]. The value of F and p of this developed model has been verified by mathematical model. The predicted values are greater than 95% which indicates the level of significance of the model. Also it indicates that predicted values are nearer to the experimental values.

i. Validating the experiment

Investigations are led to confirm the above created regression conditions. Three weld runs are made utilizing various estimations of WC, WS and PD other than those utilized in the structure framework, and the bead parameters are estimated utilizing a similar strategy. The outcomes acquired are satisfied and the details are displayed in Table 6.

j. Electrochemical corrosion

Electrochemical chemical corrosion tests are performed by using potentiodynamic polarization. Figure 2 shows the electrochemical corrosion setup (International Research Centre (IRC), Sathyabama Institute of Science and Technology, Chennai, India). For this test, the cladded pieces act as the working electrode, and saturated calemol electrode as a reference electrode and platinum act as an anode electrode in polarization cell at 37.5^0C. The cladded specimen of size 1 cm x 1 cm is fixed with the holder. The potentiostat is connected to the electrode to control the polarization scan rate. 0.167 mV/s scan rate used for this research. By using potentiostat, electrochemical potential is controlled, corresponding corrosion current (I_{CORR}) values and potential current (E_{CORR}) are recorded.

3. Results and discussions

a. Direct influence of welding parameters on response variables

The direct effect of welding parameters the impact of WC, WS and PD on the response variables are shown in Figure 3. Figure 3(a) shows the impact of welding parameters on penetration. Figure 3(a) exhibits that rise in WC raised the penetration, and hence decreasing of increasing the penetration of the sample mainly controlled by the WC. On the other hand, rise in WS leads to reduce the penetration, and

controlling of WS can subsequently help for the penetration control. When the PD raised, the penetration initially increased a little and after that pointedly decreased [12]. Figure 3(b) demonstrates the impact of welding parameters on reinforcement (R). It shows that rise in WC increased the reinforcement, while with an increment in WS, the reinforcement decreased. Despite evidenced the small rise in height of reinforcement with rise in PD, the impact of PD parameter during welding plays less important role on reinforcement. [12].

Figure 3 (c) explains that the WS and WC have distinguishing effect on weld bead width like reinforcement. It is clearly noticed that the width of the bead during welding raised with rise in WC. Additional deposition rate of filler wire with more fluidity might be credited for this rise the value of bead width with WC. Inspite of the fact that the PD have less impact on width (W), compared with WC and WS, width first diminishes slightly and after that increased with the additional rise of PD [13]. The form factor increases slightly and remains almost constant, when increasing the PD. This is because of the rate of rise of the reinforcement, which is lower than the width of weld bead [12]. Increasing the WS from lesser level to greater level increases the value of the form factor. The height of reinforcement and width of weld bead both reduces with increasing the WS. Particularly, height of reinforcement reduces steeper than decrease in weld bead width. Since the WS is inversely proportional to the heat input, less amount of metal melt in base metal as well as in electrode. Due to high WS, the welding gun travels more distance for same period of time. So the electrode and base metal do not have sufficient time to melt. Because of lesser time, it leads to lesser heat input, which tend to reduce the weld bead width and height of reinforcement [12].

b. **Interaction effect of welding parameters on response variables**

Figure 4 illustrates the interaction impact of welding parameters on the response variables. Figure 4(a) shows the interaction impact of welding parameters on penetration. This interaction figure confirmed that rise in WC leads to raise the penetration of the sample, at all degrees of WS. In any case, penetration of the sample rises due to rise in WS. Rising the WS rise the penetration, over the limit leads to reduce the penetration due lesser heat input. Similarly lowering the WS increase the size of the weld pool which

leads to rise the penetration. Lowering the WS further leads to cushioning impact of the weld pool which prevents the penetration of the sample [13]. Figure 4(b) displays the collaboration effect of welding parameters on width. It is clear that the bead width size reduces with rise in WS for all level of WC. The region of different weld bead width for various levels of WS and WC are showed in figure 4(b), which demonstrates that, size of the weld bead rises with rising WC and WS [14]. Figure 4(c) shows the interaction effect of welding parameters on reinforcement. From Figure 4(c), it is very well seen that the reinforcement rises with rise in WC for all level of WS, However, it is obvious that the reinforcement decreases with increase in WS for all level of WC [14]. Increasing WC leads to decrease in form factor from lowest current value to higher current value. The ratio width of the bead to height of reinforcement is form factor. This means beads of the width decreases and height of reinforcement increases when WC increases. Increasing the WC leads to more amount of heat input to weld electrode and the base metal to melt. Furthermore, more amount of heat increases the momentum of the molten droplets, which strikes the weld pool causing the penetration. Hence, the width of the weld bead decreases and the height of reinforcement increases. But the value of form factor increases quickly at high level of WS, and reduces gradually at low level of WS [12].

c. Microstructural studies

The figure 5(a), (b) and (c) show the microstructures of the base metal before and after cladding of ER NiCr-3 and Stellite 6. It is clear that the FCC austenitic phase in ER NiCr 3 composed of coarse equiaxed austenite grains, which propagates from the heat affected zone (HAZ). The ERNiCr 3 molten metal solidified quicker, and it forms the complex grains because of different alloying components, such as, Ni and Cr, which gives the good corrosion resistance and the ability to withstand at higher temperature. The ERNiCr 3 solidifies in the phases of δ and γ of Fe, which, on slow cooling, sets as austenite, and the microstructure is composed of ferrite in austenitic dendrites. Chromium composition remains as a solute in the boundary grains, which increases the corrosion resistance of the welded metal.

The SEM images are shown in figure 6 (a), (b) and (c). From the images, it is seen that it is composed of dendrites and interdendrites, which are located in grain boundaries. The intermetallics compositions,

such as, Cobalt and Chromium, react with carbon to form the shape the fundamental carbides, which are responsible for hardness, abrasion and corrosion resistance during high temperature [2]. The presence of carbon plays an important role to improve the wear resistance by forming carbides with the metals in Co-Cr alloy by forming Cr_7C_3 carbides. If the carbon percentage is increased by 2.5% weight, then the development of carbides with these metals would be around 30% weight of the Stellite 6 composite. The size and state of the carbides are influenced by their solidification rate for various welding forms which strongly influences the hardness and strength.

The EDAX investigation has been performed for examining the variety of alloying components presents in the combination or cladding zone of hardened steel and Stellite 6. The EDAX images are shown in figure 7 (a), (b) and (C). Iron components has been dropped as it moves towards cladded surface. The percentage of iron components are varying from SA 387 Gr 91 to stellite 6 cladded surface, which leads to change in densities of iron and nickel in welded area. It is evident that ERNiCr3 diluted in stellite 6.

d. Hardness test results

The vickers hardness values shows in figure 8. The hardness values of three samples shows that the use of ERNiCr-3 and Stellite 6 increases the hardness. The vickers hardness value closer to the top layer of the stellite 6 is closer to 565.79. Because of the cobalt matrix, the value of the hardness increases to the top layer. The hardness value keep on reduces to the next subsequent layer because of dilution of the ERNiCr-3. The harness value of the ERNiCr-3 had dilute with stellite 6 and SA387 Gr 91. So the dilution values changes from 236.59 closer to the stellite 6 and 230.08 closer to the base metal.

e. Electrochemical corrosion

The figure 9 shows the polarization curve between Log (I) and E for the cladded samples. The cladded specimen, which is shielded by ERNiCr-3 and Stellite 6, to enhance higher current densities than the SA 387 Gr 91. The corrosion current (I_{CORR}) values and potential current (E_{CORR}) values of the welded samples are given in table 7. The potential voltage (E_{CORR}) value for the SA387Gr 91 is -0.38 V [14] and the potential value of Stellite 6 is -0.63 V [15-17]. The results show that Stellite 6 improves the corrosion

resistance of the cladded samples. Stellite 6 exhibit. Equation 12 used to calculate the values of corrosion rate.

Corrosion rate (CR) = $0.327 \times 10^{-4} \frac{\text{Icorr} Eq}{Density}$

Where CR – Corrosion rate.

I_{corr} – Corrosion current from plot in $\frac{\mu A}{Square\ centimeter}$.

Eq – Equivalent weight

Conclusion

In this work, SA387 Gr 91 is cladded with stellite 6 as cladding material and ERNiCr-3 as a buffer layer by robotic welding, and the effects of welding speed, welding current and nozzle-to-tip distance on the mechanical and corrosion properties are investigated. The following observations are made.

- The application of ERNiCr-3 reduces the cracks and pores on the surface of the cladded metal.
- Among the chosen parameters, welding current is the most important parameter controlling the mechanical and corrosion properties.
- The interaction effects have significant influence over the weld bead geometry and their effects can't be ignored.
- The predicted values of the developed model are closer to the experimental model
- The base metal and weld metal of this sample not showed any cracks and pores in the heat affected zone and fusion zone.

From the results, it is concluded that the combination of ERNiCr-3 and Stellite 6 enhances the corrosion resistance and mechanical properties of SA387 Gr 91 significantly.

References

ArabiJeshvaghani R, Shamanian M, Jaberzadeh M, 2011. Enhancement of wear resistance of ductile iron surface alloyed by Stellite 6. Mater Design,32 (4), 2028–2033, doi:10.1016/j.matdes.2010.11.060.

Britto Joseph G, Valarmathi T. N, Mageshwaran, G, JeyaJeevahan, Sriram V, Durai Raj R. B, 2019, " Studies on the Influence of WeldingParameters in Cladding of ERNiCrMo-10 on AISI 4140 Using

GMAW Process" Lecture Notes in Mechanical Engineering, https://doi.org/10.1007/978-981-13-6374-0_67

Deng D.W, Zhang C P, Chen R, Xia H.F, 2013, Microstructure and Microhardness of 17-4PH Deposited with CobasedAlloy Hardfacing Coating" Phys. Procedia, 50,177–184, doi: 10.1016/j.phpro.2013.11.029

Rambau T. G, Popoola A. P. I, Loto C.A, MathebulaT and TheronM, 2013,Tribological and Corrosion Characterization of Al/(Stellite-6+Zirconium) Laser Alloyed Composites" Int. J. Electrochem. Sci., 8 5515 – 5528

Durairaj R.B, Ramachandran S, "In Vitro Characterization of Electrodeposited Hydroxyapatite Coatings on Titanium (Ti6AL4V) and Magnesium (AZ31) Alloys for Biomedical Application" Int. J. Electrochem. Sci., 13 (2018) 4841 – 4854, doi: 10.20964/2018.05.85

Joseph, G.B., NarendraKumar, G., Mageshwaran, G., Jeevahan, J., Sriram, V., Durai Raj, R.B, 2018, Optimisation of process parameters for electroless nickel plating on SS316L for refrigeration systems "Int. J. Ambient Energy, pp. 1-5,DOI: 10.1080/01430750.2018.1437564

Kannan. T, Murugan N, 2006, "Effect of flux cored arc welding process parameterson duplex stainless steel clad quality" J Mater Process Tech 176, 230–239, doi:10.1016/j.jmatprotec.2006.03.157

Mohammed M. F, Kottaimathan G K, RajanbabuR, " Metallurgical Study of Stellite 6 Cladding on 309-16L Stainless Steel" Arab J SciEng, 176(1-3), 230-239, DOI 10.1007/s13369-017-2457-7.

Mohammed M F, Muthukannan D, Kottaimathan G k, RajanbabuR, 2016. Plasma Transferred Arc Welding of Stellite 6Alloy on Stainless Steel for Wear Resistance" Procedia Technology 25, 1305–1311. doi: 10.1016/j.protcy.2016.08.226

Palani P. K, Murugan N, 2006. Development of mathematical models for prediction of weld beadgeometry in cladding by flux cored arc welding" Int J Adv. Manuf. Technol. 30: 669–676, DOI 10.1007/s00170-005-0101-2

Rambau T. G, Popoola A. P. I, Loto C.A, MathebulaT and TheronM, 2013.Tribological and Corrosion Characterization of Al/(Stellite-6+Zirconium) Laser Alloyed Composites. Int. J. Electrochem. Sci., 8. 5515 – 5528.

Sandeep J, Rahul C, Narinder P Mehta, 2014. Effect of welding parameters on bead profile, microhardness and H_2contentin submerged arc welding of high-strength low-alloy steel" Proc IMechE Part B:J Engineering Manufacture, Vol 228(1) 82–94

SerkanApay, BehcetGulenc, 2014. Wear properties of AISI 1015 steel coated with Stellite 6 by microlaser welding" Mater Design, 55, 1–8.https://doi.org/10.1016/j.matdes.2013.09.056

Shekhar S, GargR.K.,2017, Process parameter optimization of gas metal arc welding on IS:2062 mild steel using response surface methodology" J. Manuf. Process. 25, 296–305.doi.org/10.1016/j.jmapro.2016.12.016

Singh V. B, Archana G, 2005. Microstructural and corrosion studies of 9Cr-1Mo steel in acidic methanol solutions" Indian journal of chemical technology, Vol.12, pp. 347-355.

Tian H. L, Wei S. C, Chen Y. X, Tong H, Liu Y, and Xu B. S 2014. " Microstructure and wear resistance of an arc-sprayed fe-based coatingafter surface remelting treatment" Strength Mater, 46(2). DOI: 10.1007/s11223-014-9540-z

Yuwen S, MingzhongHao, 2012. Statistical analysis and optimization of process parameters in Ti6Al4V laser cladding using Nd:YAGlaser" Opt Laser Eng 50.985–995.

https://doi.org/10.1016/j.optlaseng.2012.01.018

Table 1: Chemical Composition

Element	Cr	Mo	Mn	C	P	Si	S	Iron	Ni	Cu	Ti	Nb	W	Co
SA 387 Gr 91 (%)	8.3	0.96	0.36	0.07	0.02	0.26	0.01	Balance	-	-	-	-	-	-
ERNiCr3	16	3	0.5	0.09	0.021	0.68	0.03	Balance	68	0.12	0.05	2.56	-	-
Stellite 6	29	0.65	-	1.26	-	1.14	-	3.6	2.02	-	-	-	5.7	Balance

Table 2: Welding parameters ranges

Parameter	**Unit**	**Notation**	**Factor level of ERNiCr3**			**Factor level of Stellite 6**		
			-1	**0**	**1**	**-1**	**0**	**1**
Welding Current	Ampere	WC	200	220	240	160	170	180
Welding Speed	mm/min	WS	160	200	240	150	200	250
Nozzle to Plate distance	Mm	PD	17	20	23	17	20	23

Table 3: Design matrix of ER NiCr-3 &Stellite 6

Run	Welding Current	Welding speed	Nozzle to plate distance	Width	Reinforcement	Penetration	Form factor	Width	Reinforcement	Penetration	Form factor
	A	mm/min	Mm	mm	Mm	mm		mm	mm	mm	
1	0	-1	-1	9.9	4.39	0.79	2.255	9.7	4.37	0.8	2.2
2	1	-1	-1	13.27	4.79	1.11	2.77	13.29	4.81	1.1	2.77
3	-1	0	-1	8.31	4.03	0.74	2.062	8.3	4.02	0.73	2.06
4	1	0	-1	12.39	4.31	1	2.875	12.4	4.32	1.01	2.88
5	-1	-1	1	10.05	4.46	0.89	2.253	10.04	4.45	0.88	2.28
6	1	-1	0	12.34	4.73	1.11	2.609	12.35	4.74	1.12	2.58
7	-1	0	1	9.38	4.11	0.73	2.282	9.4	4.1	0.72	2.28
8	1	0	1	11.73	4.37	0.78	2.684	11.71	4.38	0.79	2.67
9	-1	0	0	9.01	4.17	0.88	2.161	9.02	4.15	0.89	2.19
10	1	0	0	11.87	4.29	0.98	2.767	11.86	4.31	0.99	2.74
11	0	-1	0	11.02	4.54	1.04	2.427	11.03	4.53	1.05	2.43
12	0	0	0	10.64	4.33	1.04	2.457	10.63	4.34	1.04	2.49
13	0	0	-1	11.25	4.33	1.03	2.598	11.27	4.32	1.03	2.56
14	-1	-1	1	10.26	4.43	0.87	2.316	10.24	4.43	0.86	2.28
15	0	0	0	10.79	4.33	1.05	2.492	10.78	4.32	1.04	2.47
16	0	0	0	10.82	4.33	1.05	2.499	10.83	4.34	1.06	2.49
17	0	-1	0	11.01	4.52	1.08	2.436	11.02	4.52	1.08	2.45

Table 4: Regression co efficient

Co efficient	Values of Co efficient							
	Width (W)		Reinforcement (R)		Pentration (P)		Form factor (FF)	
	ERNiCr-3	Stellite 6	ER iCr-3	Stellite 6	ERNiCr-3	Stellite 6	ERNiCr-3	Stellite 6
K_0	10.73	10.75	4.32	4.32	1.05	1.05	2.48	2.49
K_1	1.48	1.51	0.16	0.18	0.095	0.097	0.25	0.24
K_2	-0.42	-0.4	-0.2	-0.2	-0.061	-0.061	0.018	0.024
K_3	-0.09	-0.063	0.02	0.03	-0.034	0.038	-0.035	-0.031
K_1K_1	0.17	0.13	-0.026	-0.027	-0.012	-0.006	0.065	0.059
K_2K_2	-0.42	-0.44	-0.0083	-0.011	-0.054	-0.051	-0.094	-0.1
K_3K_3	0.18	0.158	0.009	0.0073	-0.024	-0.022	0.038	0.033
K_1K_2	-0.13	-0.15	0.017	0.019	-0.063	-0.058	-0.05	-0.052
K_1K_3	-0.076	-0.091	0.013	0.013	-0.044	-0.043	-0.021	-0.021
K_2K_3	0.36	0.37	0.052	0.052	-0.062	0.072	0.051	0.036

Table 5: ANOVA test for the welding parameters

Source	Sum of squares			Mean			F			p-value Prob> F		
	Width	Reinforceme	Penetratio	Width	Reinforceme	Penetratio	width	Reinforceme	Penetratio	width	Reinforceme	Penetration

		nt	n		nt	n		nt	n		nt	
Model(significant)	26.8	0.641	0.283	2.98	0.0713	0.031	250.3	192.13	142.4	0.001	0.0001	0.0001
WC	15.1	0.203	0.062	15.1	0.2033	0.062	1268	548.18	282.9	0.001	0.0001	0.0001
WS	1.34	0.327	0.031	1.34	0.3271	0.030	112.3	881.96	139.1	0.001	0.0001	0.0001
PD	0.02	0.005	0.008	0.02	0.0054	0.008	1.95	14.562	37.18	0.205	0.0066	0.0005
WCWS	0.12	0.005	0	0.12	0.0054	0.029	10.46	14.48	1.263	0.014	0.0067	0.2982
WCPD	1.00	0.001	0.013	1.00	0.0006	0.013	84.06	1.639	60.67	0.001	0.2412	0.0001
WSPD	0.13	0	0.003	0.13	0.0003	0.003	11.64	0.827	12.46	0.012	0.3933	0.0096
WC^2	0.04	0.001	0.006	0.04	0.0007	0.007	3.437	1.89	29.27	0.106	0.2116	0.001
PD^2	0.01	0	0.003	0.01	0.0003	0.003	1.172	0.796	14.44	0.315	0.402	0.0067
WS^2	0.28	0.006	0.011	0.28	0.0056	0.011	23.72	15.021	49.50	0.002	0.0061	0.0002
Lack of Fit (Not significant)	0.04	0.002	0.001	0.01	0.0007	0.001	1.334	5.366	0.911	0.381	0.0691	0.5107
Pure Error	0.04	0.001	0.001	0.01	0.0001	0.001						

Table 6: Results of confirmation

Results of confirmation						
Parameters of ERNiCr-3 &Stellite 6			**Response**			
I (A)	**S (mm/min)**	**D (mm)**	**W (mm)**	**R (mm)**	**P (mm)**	**FF**
220	200	20	10.64	4.33	1.04	2.46
170	200	21	10.78	4.32	1.06	2.49

Table 7: Polarization data of the cladded samples

Samples	**E_{CORR}(V)**	**I_{CORR}(μA/cm²)**	**Corrosion rate (mm/yr)**
SA387 Gr 91	-0.381	1620	0.0041
Stellite 6	-0.585	1250	0.0036

List of Tables

List of Figures

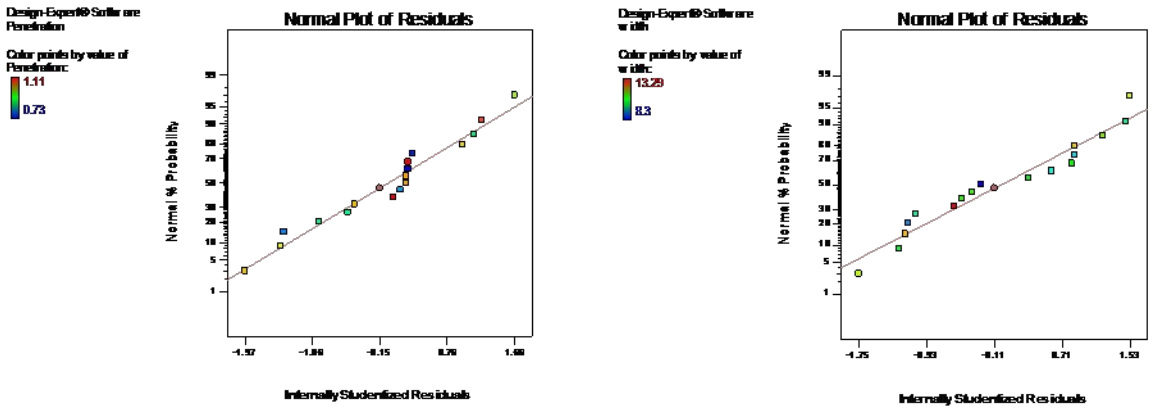

Figure 1: Scatter Diagram

Figure 2: Electrochemical corrosion

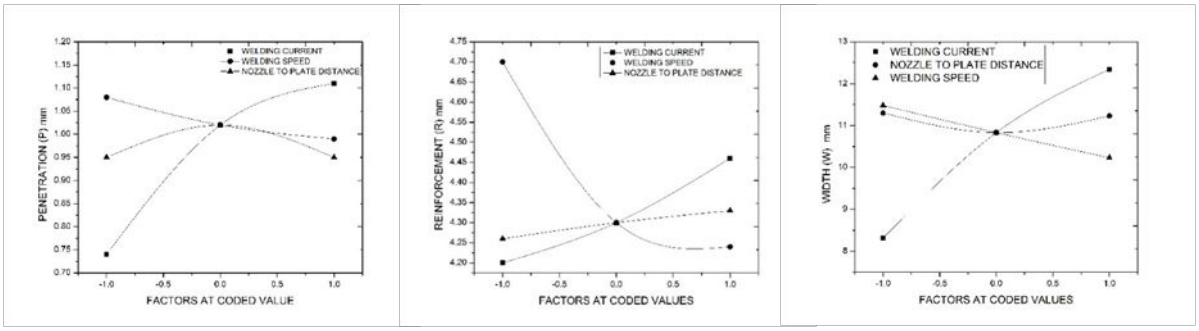

(a) (b) (c)

Figure 3 Direct effect of welding parameters on (a) penetration (b) reinforcement and (c) width

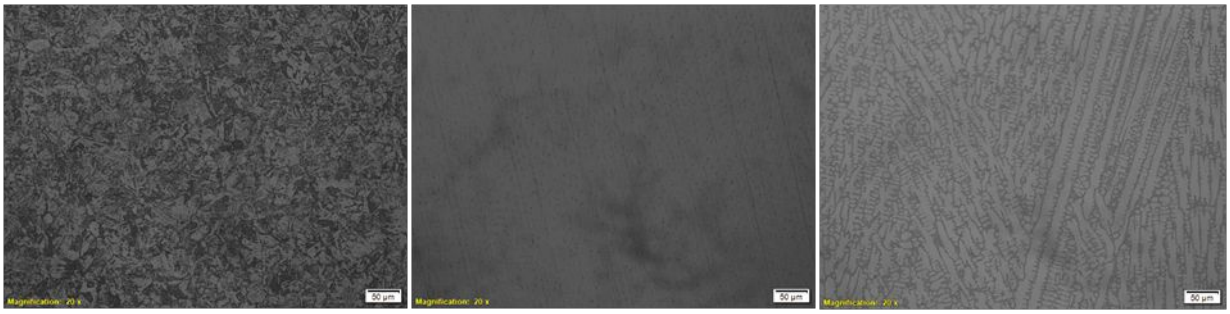

(a) (b) (c)

Figure: 5 Microstructure of (a) SA 387 Gr 91; (b) ERNiCr-3; (c) Stellite – 6

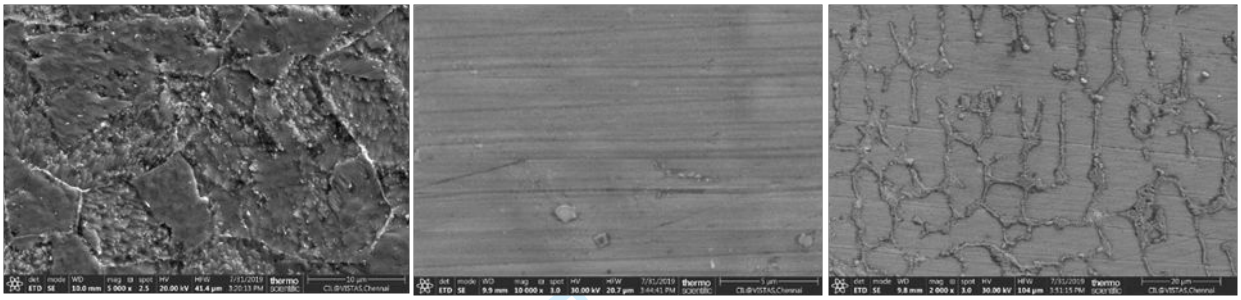

(a) (b) (c)

Figure 6:(a) SEM image of SA 387 Gr 91; (b) SEM image of ER NiCr 3; (c): SEM image of Stellite 6

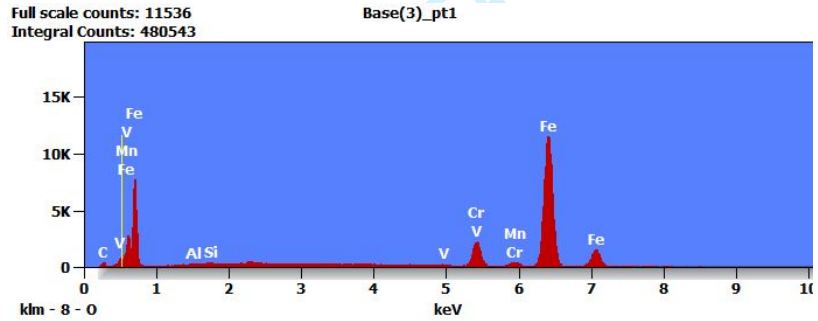

(a)

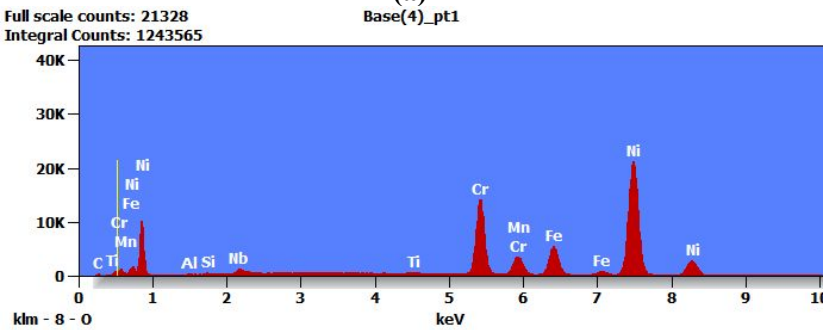

(b)

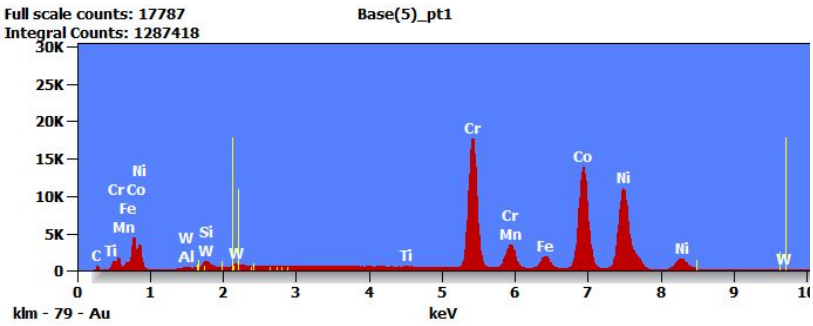

(c)

Figure 7: EDAX image of the (a) base metal (b) ERNiCr 3 (c) Stellite 6

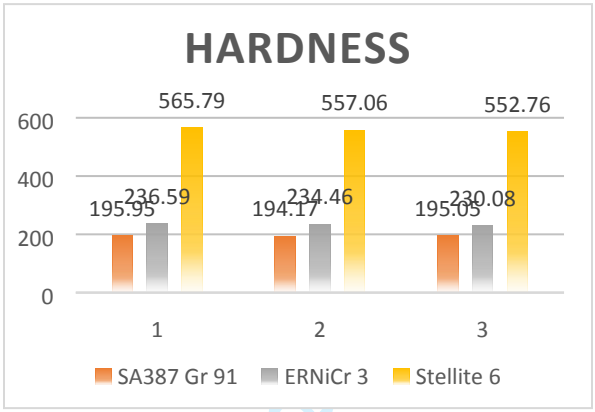

Figure 8: Hardness values

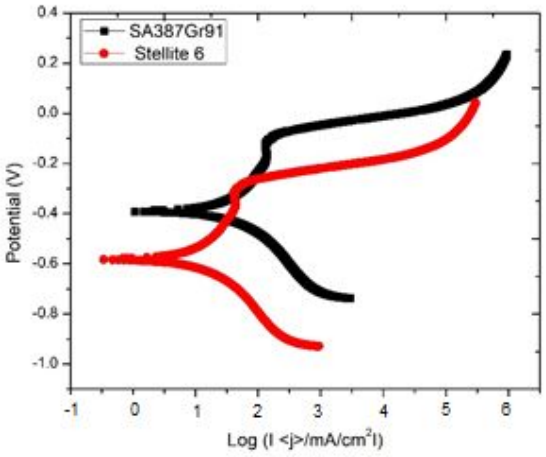

Figure 9: Electro chemical corrosion plot

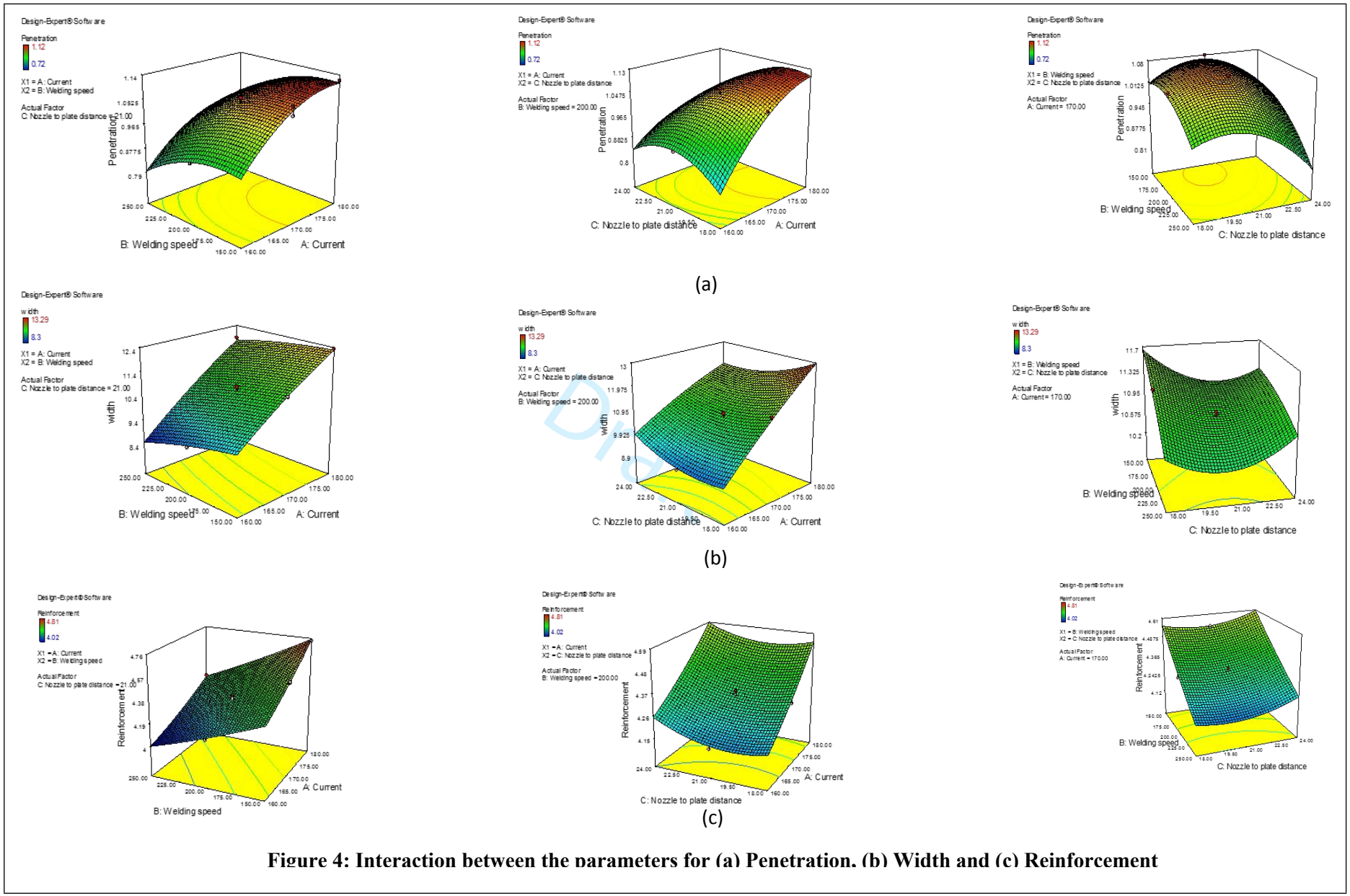

Figure 4: Interaction between the parameters for (a) Penetration, (b) Width and (c) Reinforcement